Did galaxy assembly and supermassive black-hole growth go hand-in-hand?

R.A. Windhorst [a,*], S.H. Cohen [a], A.N. Straughn [a], R.E. Ryan Jr. [a],
N.P. Hathi [a], R.A. Jansen [a], A.M. Koekemoer [b], N. Pirzkal [b], C. Xu [b],
B. Mobasher [b], S. Malhotra [b], L. Strolger [b], J.E. Rhoads [b]

[a] *Department of Physics and Astronomy, Arizona State University, Tyler Mall PSF-470, Box 871504, Tempe, AZ 85287, United States*
[b] *Space Telescope Science Institute, Baltimore, MD 21218, United States*

Abstract

In this paper, we address whether the growth of supermassive black-holes has kept pace with the process of galaxy assembly. For this purpose, we first searched the Hubble Ultra Deep Field (HUDF) for "tadpole galaxies", which have a knot at one end plus an extended tail. They appear dynamically unrelaxed—presumably early-stage mergers—and make up $\sim$6% of the field galaxy population. Their redshift distribution follows that of field galaxies, indicating that—if tadpole galaxies are indeed dynamically young—the process of galaxy assembly generally kept up with the reservoir of field galaxies as a function of epoch.

Next, we present a search for HUDF objects with point-source components that are optically variable (at the $\gtrsim 3.0\sigma$ level) on time-scales of weeks–months. Among 4644 objects to $i'_{AB} \simeq 28.0$ mag (10σ), 45 have variable point-like components, which are likely weak AGN. About $\sim$1% of all field objects show variability for $0.1 \lesssim z \lesssim 4.5$, and their redshift distribution is similar to that of field galaxies. Hence, supermassive black-hole growth in weak AGN likely also kept up with the process of galaxy assembly. However, the faint AGN sample has almost no overlap with the tadpole sample, which was predicted by recent hydrodynamical numerical simulations. This suggests that tadpole galaxies are early-stage mergers, which likely preceded the "turn-on" of the AGN component and the onset of visible point-source variability by $\gtrsim 1$ Gyr.
© 2006 Elsevier B.V. All rights reserved.

Keywords: Galaxies: mergers; Galaxies: formation; Galaxies: Active Galactic Nuclei; Supermassive black holes

Contents

* Corresponding author. Tel.: +1 480 965 7143/3561.
  E-mail address: rogier.windhorst@asu.edu (R.A. Windhorst).

1. Introduction

From the WMAP polarization results (Kogut et al., 2003), population III stars likely existed at $z \simeq 20$. These massive stars ($\gtrsim 250\ M_\odot$) are expected to produce a large population of black holes (BH; $M_{bh} \gtrsim 150\ M_\odot$; Madau and Rees, 2001). Since there is now good dynamical evidence for the existence of supermassive ($M_{bh} \simeq 10^6$–$10^9\ M_\odot$) black holes (SMBH's) in the centers of galaxies at $z \simeq 0$ (Kormendy and Richstone, 1995; Magorrian et al., 1998; Kormendy and Gebhardt, 2001), it is important to understand how the SMBH's seen at $z \simeq 0$ have grown from lower mass BH's at $z \simeq 20$. A comprehensive review of SMBH's is given by Ferrarese and Ford (2004). One suggestion is that they "grow" through repeated mergers of galaxies, which contain less massive BH's, so the byproduct is a larger single galaxy with a more massive BH in its center. The growth of this BH may then be observed via its AGN activity. If this scenario is valid, there may be an observable link between galaxy mergers and increased AGN activity (Silk and Rees, 1998). Therefore, studying this link as a function of redshift could give insight into the growth of SMBH's and its relation to the process of galaxy assembly.

Recent numerical simulations addressed some long-standing issues in the dissipational collapse scenario (White and Rees, 1978) by including previously-neglected energetic feedback from central SMBH's during the merging events (e.g., Robertson et al., 2005). They emphasize the relationship between the central BH mass and the stellar velocity dispersion, which confirms the link between the growth of BH's and their host galaxies (di Matteo et al., 2005; Springel et al., 2005a,b). The present study provides observational support for these models at cosmological redshifts.

2. The hubble ultra deep field data

The Hubble Ultra Deep Field (HUDF; Beckwith et al., 2006) is the deepest optical image of a slice of the Universe ever observed. It consists of 400 orbits with the HST advanced camera for surveys (ACS) observed over a period of 4 months in four optical bands ($BVi'z'$). These are supplemented in the JH-bands with the near-infrared camera and multi-object spectrograph (NICMOS; Bouwens et al., 2004). The HUDF reaches ~ 1.0 mag deeper in B and V and ~ 1.5 mag deeper in i'_{AB} and z'_{AB} than the equivalent filters in the Hubble Deep Field (HDF, Williams et al., 1996).

A large number of galaxies in the HUDF appear dynamically unrelaxed, which suggests they must play an important role in the overall picture of galaxy formation and evolution. In particular, we notice many galaxies with a knot-plus-tail morphology, which constitute a well-defined subset of the irregular and peculiar objects in the HUDF that is uniquely measurable. According to di Matteo et al. (2005), this morphology appears to represent an *early* stage in the merging of two nearly-equal mass galax-

ies. They are mostly linear structures, resembling the "chain" galaxies first reported by Cowie et al. (1995). When more than two clumps come together, these objects may be more akin to the luminous diffuse objects and clump clusters (Conselice et al., 2004; Elmegreen et al., 2004a,b), or other types of irregular objects (Driver et al., 1995; van den Bergh, 2002).

Since the HUDF data were observed over a period of 4 months, it also provides a unique opportunity to search for variability in all types of objects to very faint flux levels, such as faint stars, distant supernovae (SNe), and weak active galactic nuclei (AGN). From all objects detected in the HUDF, we therefore selected the subset of tadpole galaxies and variable objects, and analyzed their properties in the i'_{AB}-band, where the HUDF images are deepest and have the best temporal spacing over 4 months. Yan and Windhorst (2004) discuss how the i'_{AB}-selection result in a small bias against objects at $z \gtrsim 5.5$ in the high redshift tail of the redshift distribution. However, tadpole galaxies at $z \simeq 5.5$ *do* exist (e.g., Rhoads et al., 2005). Since most HUDF objects have $z \gtrsim 1.5$, the i'_{AB}-band images sample the rest-frame UV, where AGN are known to show more variability (Paltani and Courvoisier, 1994).

To address whether supermassive black-hole growth kept pace with galaxy assembly, we will present in this paper the redshift distribution of both tadpole galaxies and weak variable AGN in the HUDF, and compare these with the redshift distribution of the general field galaxy population.

3. Tadpoles as proxy to galaxy assembly

The steps to select galaxies with the characteristic "tadpole" shape are described in Straughn et al. (2006). In short, objects of interest have a bright "knot" at one end and an extended "tail" at the other. Two different source catalogs were made to $i'_{AB} = 28.0$ mag using SExtractor (Bertin and Arnouts, 1996): a highly deblended catalog containing many point-like sources, including the knots of potential tadpole galaxies, and a low-deblending catalog containing extended sources, including the tadpole's tails.

First, the knots of the tadpole galaxies were selected by setting an axis-ratio limit. "Knots" were defined from the highly deblended catalog with an axis ratio rounder than some critical value ($b/a > 0.70$). "Tails" are elongated objects selected from the low-deblending catalog with $b/a < 0.43$. Tadpoles were defined when a knot was within a certain distance of the geometrical center of a tail, namely $<4a$ (in semi-major axis units of the tail). We also required that the knot be $>0.1a$ from the tail's geometrical center, since we are searching for asymmetric objects, and want to eliminate upfront as many of the true edge-on mid-type spiral disks as possible. The tadpole candidates also must have the knot near one end of the tail, hence we selected only those tails and knots with a relative position angle $\Delta\theta \leqslant 20°$, as measured from the semi-major axis of the tail.
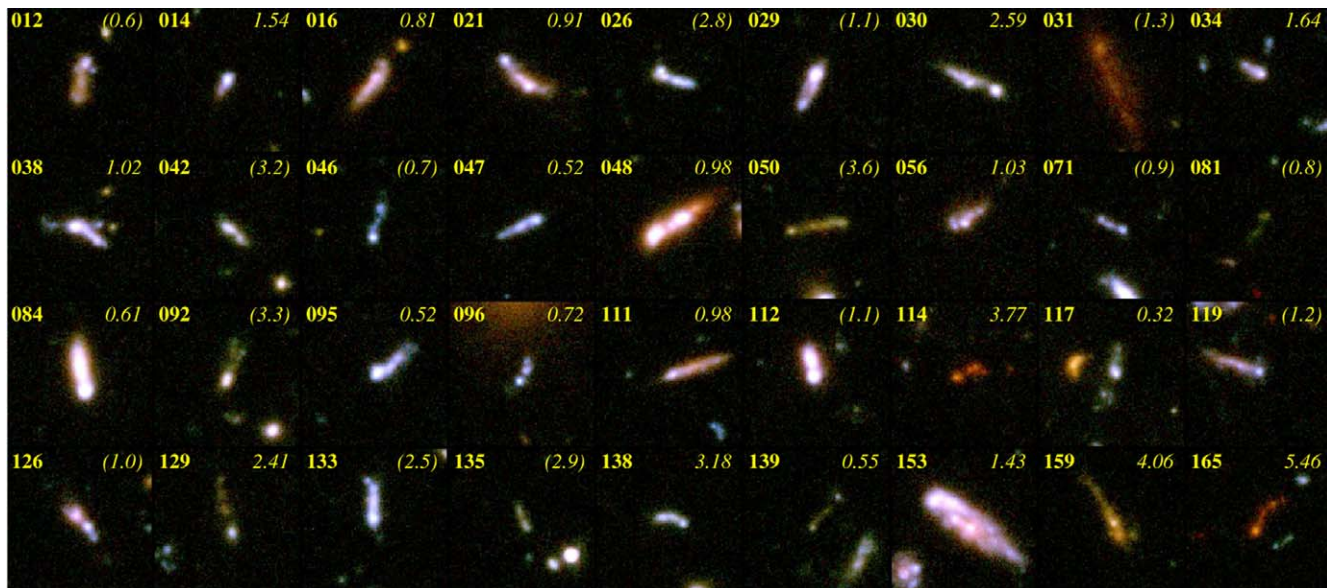
Fig. 1. i'_{AB}-Band mosaic of a subset of the HUDF tadpole galaxy sample. Stamps are 3 arcsec on a side. The vast majority of our tadpole sample contains the distinctive knot-plus-tail morphology.
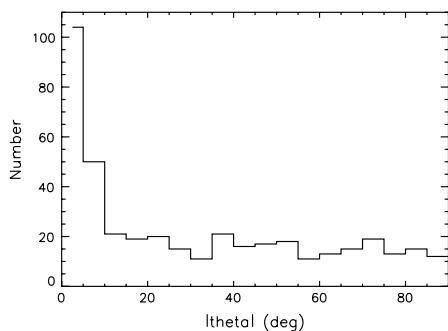

Fig. 2. Position angle (θ) distribution of all off-centered knots found within $r \leqslant 4a$ ($\lesssim 2''$) from the center of each elongated diffuse HUDF object. There is a clear excess of knots near $|\Delta\theta| \simeq 0°$, confirming the linear structure of most tadpoles.

Fig. 3b. Percentage of total galaxies that are tadpoles vs. photometric redshift. Within the statistical errors, ~6% of all galaxies are seen as tadpoles at all redshifts.

This prevented including knots and tails that appear close together on the image, but are not physically part of the same galaxy.
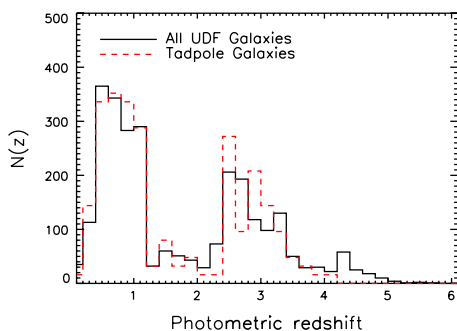

Fig. 3a. Photometric redshift distribution of galaxies in the HUDF. The solid black histogram shows the redshift distribution of all HUDF field galaxies to $i'_{AB} = 28.0$ mag, while the dashed red histogram shows the redshift distribution of the tadpole galaxies, multiplied by 16 for best comparison.
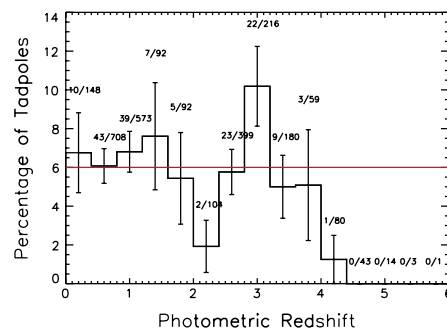
Our final sample contains 165 tadpole galaxies, a subset of which is shown in Fig. 1. These were selected from 2712 objects in the low-deblending HUDF catalog to $i'_{AB} = 28.0$ mag. Less than 10% of the selected tadpoles appear as normal edge-on disk galaxies. Fig. 2 shows a significant overabundance of knots near the end of the elongated diffuse structures ($\Delta\theta \lesssim 10°$) as compared to randomly distributed knots. Hence, the majority of tadpoles are not just chance alignments of unrelated knots. Instead, we believe they are mostly linear structures, which are undergoing recent mergers. Their redshift distribution is shown in Figs. 3a and 3b.

4. Faint variable objects as proxy to SMBH growth

Our HUDF variable object study is described in Cohen et al. (2006). Individual cosmic-ray (CR) clipped images and weight maps were used with *multidrizzle* (Koekemoer et al., 2002) to create four sub-stacks of approximately

equal exposure times that cover 0.4–3.5 months timescales. These used the same cosmic-ray maps and weight maps as the full-depth HUDF mosaics. All four epochs were *drizzled* onto the *same* output pixel scale ($0\rlap{.}''030$/pixel) and WCS frame as the original HUDF. Since we are searching for any signs of variability, we used a liberal amount of object deblending in the SExtractor catalogs, which used a 1.0σ detection threshold and a minimum of 15 connected pixels (i.e., ~the PSF area) above sky. This allows pieces of merging galaxies to be measured separately, to increase the chance of finding variable events in point-source components. Since each of the four epoch stacks have half the S/N-ratio of the full HUDF, the sample studied for variability contains 4644 objects to $i'_{AB} \lesssim 28.0$ mag ($\gtrsim 10\sigma$).

The ACS/WFC PSF varies strongly with location on the CCD detectors, and with time due to orbital "breathing" of the HST optical telescope assembly. Hence, we *cannot* use small PSF-sized apertures to search for nuclear variability, as could be done by Sarajedini et al. (2003a) for the much larger WFPC2 pixel-size and the *on-axis* location of the WFPC2 camera. Instead, we had to use *total* magnitudes of the highly deblended ACS objects. Even though
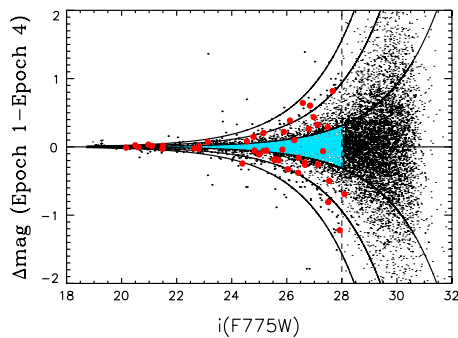
our total flux apertures may encompass the whole galaxy, any variability must come from a region less than the $0\rlap{.}''084$ PSF in size, due to the light-travel time across the variability region.

The four epoch catalogs were compared to each other, resulting in six diagrams similar to Fig. 4a, which show the change in measured total magnitudes in matched apertures as a function of the full-depth HUDF flux. The flux-error distribution was determined iteratively for each pair of observations, such that 68.3% of the points lie within the boundaries of the upper and lower 1.0σ lines that represent the Gaussian error distribution (Fig. 4a). In order to demonstrate the Gaussian nature of this error distribution at all flux levels, the Δmag-data were divided by the 1.0σ model line, and histograms were computed for the resulting normalized Δmag data at various flux-levels in Fig. 5. These histograms are well fit by normalized Gaussians with $\sigma \simeq 1.0$. The HUDF noise distribution is not perfectly Gaussian, but with 288 independent exposures in the i'_{AB}-band, the error distribution is as close to Gaussian as seen in any astronomical CCD application. Once the $\pm 1.0\sigma$ lines were determined, we find all objects that are at least 3.0σ outliers. Most outliers in Fig. 5 at Δmag $\gtrsim 3.0\sigma$ are due to object variability, after pruning large objects without visible point sources which suffered from SExtractor deblending errors. In

Fig. 4a. Magnitude difference between two HUDF epochs of all objects vs. i'_{AB}-band flux from matched total apertures. The $\pm 1\sigma$, $\pm 3\sigma$, $\pm 5\sigma$ lines are shown. Blue points show the $|\Delta$mag$| \lesssim \pm 1.0\sigma$ points used to normalize the error distribution. Large red points show the "best" 45 variable candidates from all six possible epoch combinations, many of which were seen at $\gtrsim 3.0\sigma$ in two or more epoch combinations.
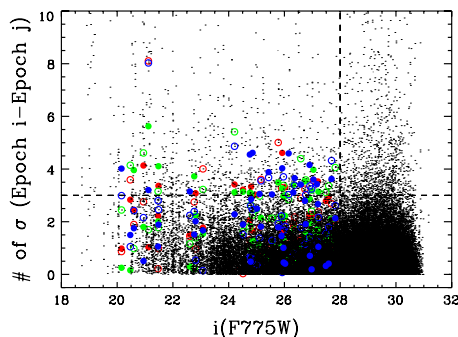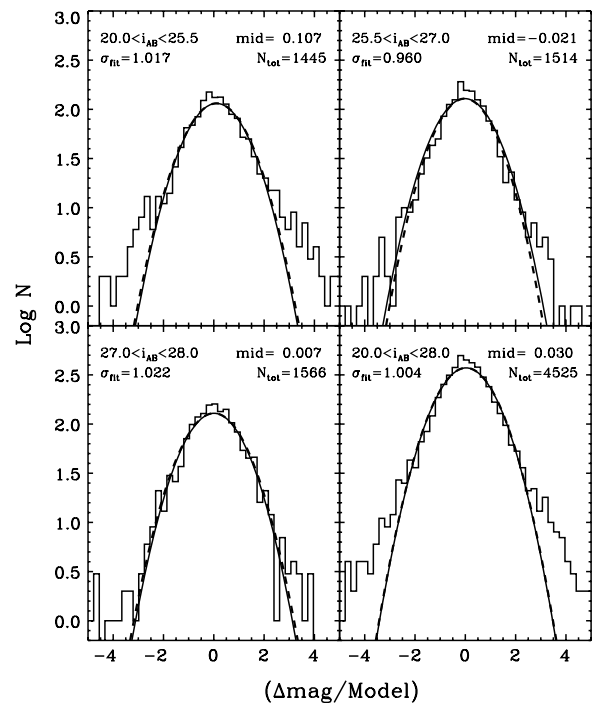

Fig. 4b. Number of σ that each object varies for all six possible epoch combinations. Colored symbols indicate the "best" sample of 45 variable candidates from Fig. 4a, that are unaffected by local image deblending issues or weight map structures. Each object appears six times in this plot.

Fig. 5. Gaussian nature of the HUDF total-flux error distribution at all flux levels. The Δmag data from Fig. 4a were divided by the best-fit model 1.0σ lines. Histograms for the indicated magnitude ranges are well fit by normalized Gaussians (parabolas in log space) with $\sigma \simeq 1.0$. The almost indistinguishable dashed and solid lines are for the best-fit σ (indicated in the legends) and for assumed $\sigma \equiv 1$ Gaussians, respectively. Hence, Fig. 5 shows that 3.0σ really means $3.0 \pm 0.1\sigma$. All objects with Δmag $\gtrsim 3.0\sigma$ not affected by deblending errors are variable candidates.
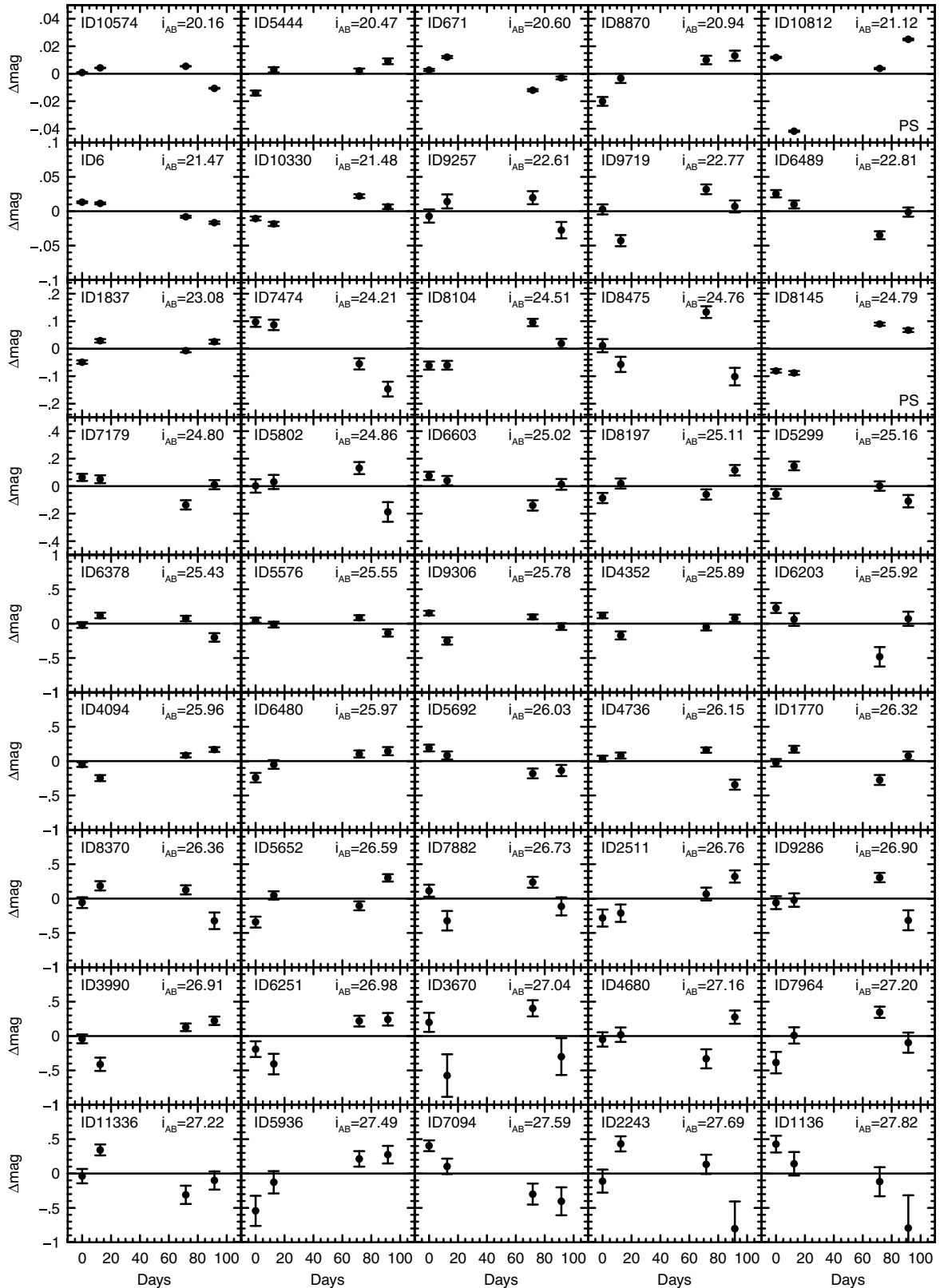
Fig. 6. Light-curves of the 45 best candidates with signs of optical point-source variability. The change in measured total flux (average-individual epoch) is plotted vertically, and the number of days since the first epoch is plotted horizontally.

Fig. 4a, we show the $\pm 1\sigma$, $\pm 3\sigma$, and $\pm 5\sigma$ lines, along with the actual data. The choice of 3.0σ implies that we should expect 0.27% random contaminants.

In total, we find 45 out of 4644 objects that show the signatures of AGN variability. These are variable at the $\gtrsim 3.0\sigma$ level, have a compact region indicative of a point

source, and are devoid of visible image defects or object splitting issues. Less than one of these 45 is expected to be a random contaminant. In total, 577 candidates were rejected due to crowding or splitting issues, or due to the lack of a visible point source. Fig. 4b shows the number of σ by which each object varied for each of the 6 possible epoch-pairs. The colored symbols are for the 45 "best" candidates. Another 57 objects were found that are "potentially" variable candidates. The four-epoch light-curves for these 45 variable candidates are shown in Fig. 6. Of these, 49% were discovered from a single epoch-pair (usually indicative of a global rise or decline as a function of time in the light-curve), 43% in two epoch-pairs, and only 5% (2 objects) in 3 epoch-pairs. Further details are given in Cohen et al. (2006). In summary, the variability fraction on a timescale of few months (rest-frame timescale few weeks to a month) is at least 1% of all HUDF field galaxies.

Since the HUDF is in the Chandra deep field-south (CDF-S, Rosati et al., 2002), there exists deep X-ray data. Within the HUDF, there are 16 Chandra sources (Koekemoer et al., 2006), and we detect four of these as variable in the optical. One of these is a mid-type spiral with $i'_{AB} \simeq 21.24$ mag, that belongs to a small group of interacting galaxies. Two others are optical point sources with $i'_{AB} \simeq 21.12$ mag and $\simeq 24.79$ mag, showing little or no visible host galaxy. Both have measured spectroscopic AGN emission-line redshifts at $z \simeq 3$ (Pirzkal et al., 2004). The detection of 25% of the Chandra sources as optically variable in the HUDF data shows that the variability method employed here is a reliable way of finding the AGN that are not heavily obscured.

The faint object variability in the HUDF is most likely due to weak AGN, given the timescales and distances involved. Strolger and Riess (2006) found only one moderate redshift SN in the HUDF, so SNe cannot be a significant source of contamination in our sample. Several other possible source of incompleteness in the variability study must be addressed. Non-variable AGN, or AGN that only vary on timescales much longer than 4 months, or optically obscured AGN would not have been detected with our UV–optical variability method. Sarajedini et al. (2003a,b) had two HDF epochs 5–7 years apart, and found 2% of the HDF objects to be variable. It is thus possible that our sampled times-scale shorter than 4 months missed a factor $\gtrsim 2$ of all AGN—the ones variable on longer time-scales.

5. The redshift distribution of tadpole galaxies and faint variable objects

We calculate photometric redshifts of all HUDF galaxies to $i'_{AB} = 28.0$ mag ($\gtrsim 20\sigma$) from the $BVi'z'$ photometry using HyperZ (Bolzonella et al., 2000), plus NICMOS JH (Thompson et al., 2005) and VLT ISAAC K-band images where available. When compared to published spectroscopic redshifts for 70 CDF-S objects (Le Févre et al.,

2005), our photometric redshifts z's have an rms scatter of 0.15 in $\delta = (\text{photo-z} - \text{spec-z})/(1 + \text{spec-z})$ if all 70 objects are included, and 0.10 in δ when we reject a few of the most obvious outliers.

The redshift distribution of all HUDF galaxies (solid line in Fig. 3a) is as expected, with the primary peak at $z \lesssim 1.0$ and a generally declining tail at $z \simeq 4$–5. These trends were also seen in the HDF field galaxies (Driver et al., 1998). A deficit of objects is apparent at $z \simeq 1$–2 due to the lack of UV spectral features crossing the $BViz(+JH)$ filters. Unlike the HDF (Williams et al., 1996), this deficit occurs because the HUDF does not yet have deep enough F300W or U-band data. The resulting redshift bias, however, is the *same* for both tadpoles, variable objects and the field galaxy population, and so divides out in the subsequent discussion. Within the statistical uncertainties in Fig. 3a, the shape of the tadpole galaxy redshift distribution follows that of the field galaxies quite closely. This suggests that if tadpole galaxies are indeed dynamically young objects related to early-stage mergers,
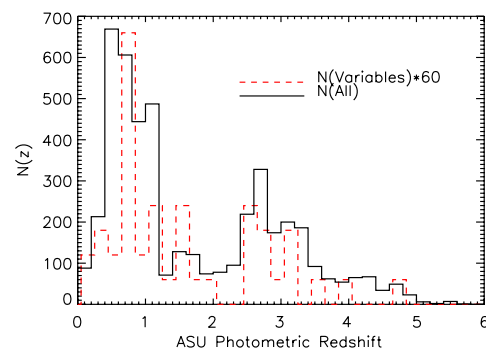

Fig. 7a. Photometric redshift distribution of all HUDF field galaxies to $i'_{AB} \lesssim 28.0$ mag (solid line), and for the "best" variable candidates (red dashed line) multiplied by 60× for best comparison. The redshift distribution of the variable objects follows that of field galaxies in general (For interpretation of the references to color in this figure legend, the reader is referred to the web version of this article.).
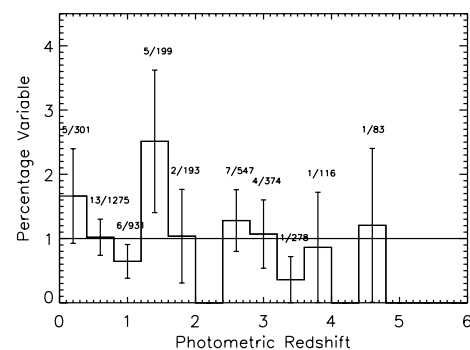

Fig. 7b. Percentage of HUDF objects to $i'_{AB} \lesssim 28.0$ AB-mag showing variable point sources as a function of redshift. Within the statistical uncertainties, about 1% of all HUDF galaxies show point source variability over the redshift range surveyed ($0 \lesssim z \lesssim 5$). Hence, SMBH growth as traced by the weak AGN fraction keeps pace with galaxy assembly as traced by the tadpoles in Fig. 3b.

they seem to occur in the same proportion to the field galaxy population at all redshifts. Tadpole galaxies may therefore be good tracers of the galaxy assembly process. The ratio of the two redshift distributions $N(z)$ and the resulting percentage of tadpole galaxies is plotted in Fig. 3b. Overall, the percentage of tadpole galaxies is roughly constant at $\sim$6% with redshift to within the statistical errors for the redshifts sampled (0.1 $\lesssim z \lesssim$ 4.5).

In Fig. 7a, we show the photometric redshift distribution for all HUDF objects with $i'_{AB} \lesssim$ 28.0 mag, and for our best 45 variable candidates. Their redshift distribution follows that of the field galaxies in general, i.e., there is no redshift where faint object variability was most prevalent. We plot in Fig. 7b the ratio of the $N(z)$ for variable objects to that of field galaxies, and show that the weak variable AGN fraction is roughly constant at approximately 1% over all redshifts probed in this study.

6. Discussion and conclusions

The fact that about 6% of all field galaxies are seen in the tadpole stage is an important constraint to hierarchical simulations. Springel et al., 2005a,b predict a tadpole-like stage $\sim$0.7–1.5 Gyr after a major merger begins, suggesting that the tadpole morphology represents an early-merger stage of two galaxies of roughly comparable mass. If this 6% indicates the fraction of time that an average galaxy in the HUDF spends in an early-merger stage during its lifetime, then every galaxy may be seen temporarily in a tadpole stage for $\sim$0.8 Gyr of its lifetime, and may have undergone $\sim$10–30 mergers during its lifetime (Straughn et al., 2006). More complex mergers involving multiple components may lead to irregular/peculiar and train-wreck type objects, and the luminous diffuse objects or clump-clusters, which dominate the galaxy counts at faint magnitudes (Driver et al., 1998). Given that tadpoles only trace a certain type and stage of merging galaxies, the above statistics are a lower limit on the number of all mergers.

The question arises, if tadpole galaxies and objects with point-sources that show signs of variability are drawn from the same population. Among our 165 tadpole galaxies, none coincide with the sample of 45 variable objects or with the CDF-S X-ray sources S (Alexander et al., 2003). At most one or two of the variable candidates resemble the tadpole galaxies of Straughn et al. (2006).

A factor of three of all AGN may have been missed, since their UV–optical flux was obscured by a dust-torus. In the AGN unification picture, AGN cones are two-sided and their axes are randomly distributed in the sky, so that an average cone opening-angle of ω implies that a fraction $1 - \sin(\omega)$ of all AGN will point in our direction. If $\omega \simeq 45°$ (e.g., Barthel, 1989, 1994), then every optically detected AGN (QSO) represents 3–4 other bulge-dominated galaxies, whose AGN reflection cone did not shine in our direction. Hence, their AGN may remain obscured by the dust-torus. Such objects could be visible to Chandra in X-rays or to Spitzer in the mid-IR, although the available Chandra and Spitzer data are not deep enough to detect all HUDF objects to AB $\simeq$ 28 mag.

Together with the factor of $\gtrsim$ 2 incompleteness in the HUDF variability sample due to the limited time-baseline sampled thus far, the actual fraction of weak AGN present in these dynamically young galaxies may thus be a factor of $\gtrsim$ 6–8$\times$ larger than the 1% variable AGN fraction that we found in the HUDF. Hence, perhaps as many as $\gtrsim$ 6–8% of all field galaxies may host weak AGN, only $\sim$1% of which we found here, and another $\gtrsim$ 1% could have been found if longer time-baseline had been available. Another factor of 3–4 of AGN are likely missing because they are optically obscured, The next generation of X-ray and IR telescopes (Windhorst et al., 2006a,b) and longer optical time-baselines are needed to detect all weak AGN in the HUDF.

Recent state-of-the-art hydrodynamical models (di Matteo et al., 2005; Springel et al., 2005a,b; Hopkins et al., 2005) suggest that during (major) mergers, the BH accretion rate peaks considerably *after* the merger started, and *after* the star-formation rate (SFR) has peaked. Their models suggest that, for massive galaxies, a tadpole stage is seen typically about 0.7 Gyr after the merger started, but $\sim$1 Gyr before the SMBH accretes most of its mass, which is when the galaxy displays strong visible AGN activity. Since the lifetimes of QSO's and radio-galaxies are known to be $\lesssim$(few $\times$ 10^7)–10^8 years (Martini, 2004; Grazian et al., 2004; Jakobsen et al., 2003), these models thus imply that the AGN stage is expected to occur considerably (i.e., $\gtrsim$ 1–1.5 Gyr) *after* the early-merger event during which the galaxy is seen in the tadpole stage.

The observed lack of overlap between the HUDF tadpole sample and the weak variable AGN sample thus provides observational support for this prediction. Hopkins et al. (2005) have quantified the timescales that quasars will be visible during merging events, noting that for a large fraction of the accretion time, the quasar is heavily obscured. In particular, their simulations show that during an early merging phase—our observed tadpole phase—the intrinsic quasar luminosity peaks, but is completely optically obscured. Only after feedback from the central quasar clears out the gas, will the object become visible as an AGN. This should be observable by Spitzer in the mid-IR as a correspondingly larger fraction of IR-selected obscured faint QSO's. To study the relation between galaxy assembly and SMBH growth in detail, we need deeper surveys at longer wavelengths with the James Webb Space Telescope (JWST; Windhorst et al., 2006a). The JWST photometric *and* PSF stability are crucial for this, since many of our HUDF objects show significant variability of less than a few percent in total flux.

Acknowledgement

References

Alexander, D.M. et al., 2003. AJ 126, 539.

Barthel, P.D., 1989. ApJ 336, 606.

Barthel, P.D., 1994. In: Bicknell, G.V., Dopita, M.A., Quinn, P.J. (Eds.), The First Stromlo Symposium on The Physics of Active Galaxies, ASP Conf. Ser., vol. 54, p. 175.

Beckwith, S. et al., 2006. AJ. (in press).

Bertin, E., Arnouts, S., 1996. A&AS 117, 363.

Bolzonella, M. et al., 2000. A&A 363, 476.

Bouwens, R.J. et al., 2004. ApJL 616, 79.

Cohen, S.H., Ryan Jr., R.E., Straughn, A.N., Hathi, N.P., Windhorst, R.A., Koekemoer, A., et al., 2006. ApJ 639, 731.

Conselice, C. et al., 2004. ApJL 600, L139.

Cowie, L., Hu, E., Songaila, A., 1995. AJ 110, 1576.

di Matteo, T. et al., 2005. Nature 433, 604.

Driver, S.P. et al., 1995. ApJL 449, L23.

Driver, S.P. et al., 1998. ApJL 496, L93–L97.

Elmegreen, D. et al., 2004a. ApJL 604, L21.

Elmegreen, D. et al., 2004b. ApJ 603, 74.

Ferrarese, L., Ford, H., 2004. SSRv 116, 523.

Grazian, A. et al., 2004. AJ 127, 592.

Hopkins, P. et al., 2005. ApJL 625, L71.

Jakobsen, P. et al., 2003. A&A 397, 891.

Koekemoer, A.M. et al., 2002. HST Calibration Workshop. In: Arribas S., et al. (Ed.). STScI, Baltimore, p. 339.

Koekemoer, A.M. et al., 2006. in preparation.

Kogut, A. et al., 2003. ApJS 148, 161.

Kormendy, J., Gebhardt, K., 2001. In twentieth Texas symposium. AIP Conf. Proc. 363, 586.

Kormendy, J., Richstone, D., 1995. ARA&A 33, 581.

Le Févre, O. et al., 2005. A&A 439, 845.

Madau, P., Rees, M., 2001. ApJ 551, L27.

Magorrian, J. et al., 1998. AJ 115, 2285.

Martini, P., 2004. In: Co-evolution of Black Holes and Galaxies. Cambridge University Press, Cambridge, p. 170.

Paltani, S., Courvoisier, T.J.-L., 1994. A&A 291, 74.

Pirzkal, N. et al., 2004. ApJS 154, 501.

Rhoads, J.E. et al., 2005. ApJ 621, 582.

Robertson, B. et al., 2005. (astro-ph/0503369).

Rosati, P. et al., 2002. ApJ 566, 667.

Sarajedini, V.L. et al., 2003a. ApJ 599, 173.

Sarajedini, V.L., 2003b. MmSAI 74, 957.

Silk, J., Rees, M., 1998. A&A 331, L1.

Springel, V. et al., 2005a. ApJ 620, 79.

Springel, V. et al., 2005b. MNRAS 361, 776.

Straughn, A.N., Cohen, S.H., Ryan Jr., R.E., Hathi, N.P., Windhorst, R.A., Jansen, R.A., 2006. ApJ 639, 724.

Strolger, L.-G., Riess, A.G., 2006. AJ 131, 1629.

Thompson, R.I. et al., 2005. AJ 130, 1.

van den Bergh, S., 2002. PASP 114, 797.

White, S.D.M., Rees, M.J., 1978. MNRAS 183, 341.

Williams, R. et al., 1996. AJ 112, 1335.

Windhorst, R.A., Cohen, S.H., Jansen, R.A., Conselice, C., Yan, H., 2006a. New Astron. Rev. 50, 113.

Windhorst, R.A. et al., 2006b. New Astron. Rev. 50, 121.

Yan, H., Windhorst, R., 2004. ApJL 612, 93.